Direct numerical simulation of elastic turbulence and its mixing-enhancement effect in a straight channel flow*

Zhang Hong-Na(张红娜)[a)b)], Li Feng-Chen(李凤臣)[a)†], Cao Yang(曹 阳)[a)], Kunugi Tomoaki[a)b)], and Yu Bo(宇 波)[c)]

[a)] *School of Energy Science and Engineering, Harbin Institute of Technology, Harbin* 150001, *China*
[b)] *Department of Nuclear Engineering, Kyoto University, Kyoto,* 606-8501, *Japan*
[c)] *Beijing Key Laboratory of Urban Oil and Gas Distribution Technology, China University of Petroleum-Beijing, Beijing* 102249, *China*

(Received 31 May 2012; revised manuscript received 30 June 2012)

In this paper, we present a direct numerical simulation (DNS) of elastic turbulence of viscoelastic fluid at vanishingly low Reynolds number ($Re = 1$) in a three-dimensional straight channel flow for the first time, using the Giesekus constitutive model for the fluid. In order to generate and maintain the turbulent fluid motion in the straight channel, a sinusoidal force term is added to the momentum equation, and then the elastic turbulence is numerically realized with an initialized chaotic velocity field and a stretched conformation field. Statistical and structural characteristics of the elastic turbulence therein are analyzed based on the detailed information obtained from the DNS. The fluid mixing enhancement effect of elastic turbulence is also demonstrated for the potential applications of this phenomenon.

Keywords: elastic turbulence, viscoelastic fluid, direct numerical simulation, mixing enhancement

PACS: 47.20.Gv, 47.27.ek, 47.27.Cn **DOI:** 10.1088/1674-1056/22/2/024703

1. Introduction

In recent years, dynamics of viscoelastic fluids and its potential applications have attracted lots of researchers to study both experimentally and numerically. A well-known example associated with viscoelastic fluid dynamics is the turbulent drag reduction realized by adding a small quantity of viscoelastic drag-reducing additives to the Newtonian solvent.[1] For a Newtonian fluid flow, the nonlinear inertial term (its strength depends on *Re,* the ratio of inertial force to viscous force) in its governing momentum equation drives the flow to be turbulent provided that the *Re* is large enough. However, in the viscoelastic fluid flow, the viscoelastic effect caused by the presence of high molecule-weight polymers or the microstructures (usually named shear-induced structures[2]) formed by surfactants in the viscoelastic solutions provides another nonlinear term, the so-called nonlinear elastic term (depending on the Weissenberg number, *Wi*, defined as the product of relaxation time of the viscoelastic fluid and the shear rate of the flow), for its governing momentum equation in addition to the nonlinear inertial term. This additional elastic effect to the turbulent flow could be regarded as the main reason for the abovementioned turbulent drag-reducing phenomenon. So far, numerous research studies from the experimental, theoretical, and numerical viewpoints (in Refs. [3]– [11], and references therein) have been carried out to clarify its intrinsic characteristics and physical mechanism. As obtained in this case, the intensive turbulent fluid motions driven by the nonlinear inertial force at a high Reynolds number are damped to a certain extent by the nonlinear viscoelastic stress.

Besides, it is noteworthy that these two nonlinear effects presented in a viscoelastic fluid flow do not necessarily coexist. This indicates another striking phenomenon generated solely by the nonlinear elastic effects. It has been verified that at an extremely low *Re* when the nonlinear inertial effect can be neglected, the nonlinear elastic effect can also result in unstable or even turbulent flow by itself, the so-called purely elastic instability or elastic turbulence. So far, purely elastic instability or elastic turbulence has been obtained and investigated mainly by experimental approaches, such as, in swirling flows between two disks,[12–14] Taylor–Couette flows[15,16] between two coaxial cylinders, and also micro-scale flows in curvilinear channels.[17,18] When *Wi* exceeds a critical threshold value, flows in these systems become unstable, showing a deviation from the laminar flow regime. With the further increase of *Wi*, some features of developed large-*Re* turbulence (or inertial turbulence), e.g., randomly fluctuating fluid motions excited in a broad range of spatial and time scales, significant increase in the rates of momentum transport and mass transport, etc., are exhibited and observed. This flow phenomenon was termed elastic turbulence and known at the beginning of this century.[12] The investigated flow configurations mentioned above[12–18] show a common feature, i.e.,

*Project supported by the Foundation for Innovative Research Groups of the National Natural Science Foundation of China (Grant No. 51121004), the National Natural Science Foundation of China (Grant No. 51076036), the Specialized Research Fund for the Doctoral Program of Higher Education of China (Grant No. 20112302110020), the Fundamental Research Funds for the Central Universities, China (Grant No. HIT.BRET1.2010008), and the Japan Society for the Promotion of Science (JSPS) Research Fellowship.

†Corresponding author. E-mail: lifch@hit.edu.cn

© 2013 Chinese Physical Society and IOP Publishing Ltd

the flow passage geometry is not always straight but with curvature, forming curvilinear streamlines at least at some locations in the flow. The presence of curvilinear streamlines in the flow was considered to be important for the occurrence of elastic turbulence.[19] It is believed that the elastic instability was caused by the additional elastic force acting on the fluids towards the direction of curvature, the so-called hoop stress, which originates from interactions between the curvilinear streamlines in the flow, and the first normal stress difference of viscoelastic solutions.[16] Elastic instability or elastic turbulence is induced when the elastic stress becomes larger than the viscous stress or dominant in the viscoelastic fluid flow.

Since the purely elastic instability or elastic turbulence is caused by the elastic stress independent of *Re*, it can thus be generated in the micro-scale areas where the *Re* is usually extremely low. Excitation of chaotic fluid motion of elastic instability or elastic turbulence could be an effective way for enhancing the mixing of fluids[17,18,20] or improving the efficiency of heat transfer in a low-*Re* flow system, such as in a microfluidic channel or lab-on-a-chip device.

Despite its great fascination to the researchers and the extensive range of potential applications in the future, the elastic instability and elastic turbulence are still poorly understood. Limited by the experimental techniques and measurements available nowadays, some detailed information, which is of great importance for investigating the flow mechanism of viscoelastic fluid, is currently difficult to obtain, such as the conformation and elastic stress tensor field. Direct numerical simulation (DNS) has been a complement to the experimental approach for any turbulent flow for many years. By directly solving the governing equations of viscoelastic flow at all the scales, all the flow information could be acquired in a detailed and complete way, which is impossible for the experimental approaches at present.

As far as we know, few numerical studies of pure elastic turbulence have been carried out. Elastic turbulence was obtained numerically for the first time by Berti *et al.*,[21] in a two-dimensional Kolmogorov flow of viscoelastic fluid. The basic phenomena observed in laboratory experiments were reproduced through numerical simulations, e.g., an increase of the drag with *Wi* and a power-law energy spectrum. A three-dimensional (3D) simulation of Kolmogorov flow of viscoelastic fluid was carried out by Zhang *et al.*,[22] finding that the elastic turbulence occurs at a smaller critical Weissenberg number Wi_c, compared with the two-dimensional case. Flow characteristics of elastic turbulence and its underlying mechanism, such as energy transfer between the solvent of viscoelastic solutions and the polymers, intermittent behavior of the turbulent flow, etc., are then analyzed and investigated.[22]

As mentioned above, almost all the studies on elastic turbulence so far have been carried out in flow systems with curvilinear streamlines, and no elastic instability or turbulence has been observed in rectilinear shear flows, except for several reports about experimental studies on transitional shear-banding flows of viscoelastic fluid in a micro-scaled rectilinear channel.[23,24] However, for the Newtonian fluid, any flow becomes unstable as long as *Re* is high enough, including rectilinear shear flow, such as Poiseille flow and plane Couette flow. Similarly, from the mathematical viewpoint, when the nonlinear elastic effect is strong enough, it is also reasonable to generate elastic turbulence at sufficiently strong enough *Wi*, in the rectilinear shear flow without curvilinear geometry, which has been verified in a 'theoretical' flow without wall effect.[21,22] However, either the polymer molecules with long chains in polymer solution or the shear induced structures in the viscoelastic surfactant solution are easy to degrade or destroy in a strong shear flow, leading to a significant reduction of the microstructures (imparting viscoelasticity to the fluid). So, it is difficult to reach a very high *Wi* required for the occurrence of elastic instability or turbulence in a rectilinear shear flow without any activating efforts in reality, resulting in the lack of observations in laboratory experiments so far.

In this paper, we present a DNS study of elastic turbulence in a 3D straight channel. This is for the first time to obtain elastic turbulence in a rectilinear shear flow with wall effect, which is realized by applying a sinusoidal force in the streamwise direction. The well-known Giesekus model is chosen for the constitutive equation for viscoelastic fluid herein. The statistical and structural characteristics of the obtained elastic turbulence, such as the velocity field information, vortex structure, conformation of microstructure, intermittent behavior of the flow, etc., are illustrated and investigated. The application of elastic turbulence in enhancement of fluid mixing is demonstrated as well. The forcing exertion manner as numerically demonstrated in the present study also provides the evidence and suggestions on how to design a physical experiment in order to elaborate the elastic turbulence phenomenon and its particular applications, such as by designing actively controlled additional devices in a rectilinear channel flow.

The rest of the present study is organized as follows. In Section 2, the numerical procedures are described in detail. Results and discussion are illustrated in Section 3 for the statistical and structural characteristics (statistics of velocity and its derivative, vortex structures, spectrum of fluctuating velocity and intermittent behaviors) of elastic turbulence and its mixing enhancement in the simulated straight channel. Conclusions drawn from the present study are summarized in Section 4.

2. Numerical simulation procedures

The 3D flow configuration for DNS of purely elastic turbulence of viscoelastic fluid at a vanishingly low *Re* is shown in Fig. 1. The x, y, and z represent the streamwise, wall-normal, and spanwise directions, and u, v, and w are the velocity components in the corresponding directions, respectively. The lengths of the computational domain in x, y, z directions are $10h$, $2h$, $5h$, respectively, where h is half the height of the channel. Periodic conditions are imposed on the boundaries of both the streamwise and spanwise directions, and for the top and bottom walls no-slip boundary conditions are adopted. The temporally random but spatially smooth feature of elastic turbulence indicates that only vortices whose sizes are large compared with the dimension of flow passage exist, which allows the utilization of coarser mesh in numerical simulations. The current simulations are conducted in a mesh with $64\times64\times64$ grids, which has been verified to be fine enough for capturing all the desired information about a very-low-*Re* elastic turbulence and is suitable for the computing resource available.

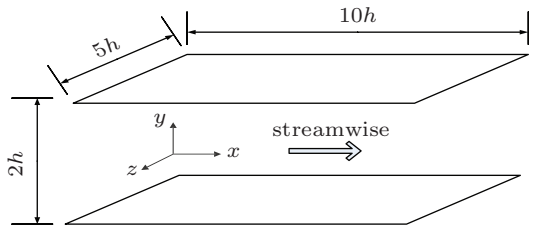


Fig. 1. Schematic plot of the flow geometry and coordinate.

In the momentum equation, a force

$$F = (F_{\mathrm{m}} \sin(2\pi y/h), 0, 0)$$

with an amplitude F_{m} is added as a source term to generate the strong rectilinear shear flows needed for inducing elastic turbulence in the channel and compensate the energy dissipation by viscous and elastic effects. Dimensionless governing equations are used. The half-height of the channel, h and the imaginary laminar velocity amplitude under the given additional force F, h/u_{l}, and ρu^2 are chosen as scales for length, velocity, time, and stress, respectively. The imaginary laminar velocity amplitude, u_{l} can be calculated by $u_{\mathrm{l}} = F_{\mathrm{m}}h^2/(4\pi^2\eta_{\mathrm{s}})$, where η_{s} is the solvent viscosity. The dimensionless governing equations describing the flow of viscoelastic fluid including continuity equation, momentum equations, and Giesekus constitutive equations are as follows:

$$\boldsymbol{\nabla}\cdot\boldsymbol{U} = 0, \tag{1}$$

$$\frac{\partial \boldsymbol{U}}{\partial t} + \boldsymbol{U}\cdot\nabla\boldsymbol{U} = -\nabla p + \frac{1}{\boldsymbol{Re}}\nabla^2\boldsymbol{U} + \frac{\beta}{\boldsymbol{ReWi}}\nabla\cdot(\boldsymbol{C}-\boldsymbol{I}) + \boldsymbol{F}^*, \tag{2}$$

$$\frac{\partial \boldsymbol{C}}{\partial t} + \boldsymbol{U}\cdot\nabla\boldsymbol{C} = \boldsymbol{C}\cdot\nabla\boldsymbol{U} + \nabla\boldsymbol{U}^{\mathrm{T}}\cdot\boldsymbol{C} - \frac{(\boldsymbol{I}+\alpha(\boldsymbol{C}-\boldsymbol{I}))\cdot(\boldsymbol{C}-\boldsymbol{I})}{Wi}. \tag{3}$$

In the simulation, β is set to be 0.5, which is the ratio of kinematic viscosity contributed by the solute (η_{P}) to that by the solvent (η_{s}); $\boldsymbol{C}$ is the dimensionless conformation tensor of the viscoelastic solution normalized by η_{P}; $\boldsymbol{I}$ is the unit tensor; α is the mobility factor of Giesekus constitutive model and set to be 0.001 in the simulation; *Re* and *Wi* are defined as $Re = u_{\mathrm{l}}h/(\eta_{\mathrm{P}}+\eta_{\mathrm{s}})$, $Wi = \lambda u_{\mathrm{l}}/h$, respectively, with λ being the relaxation time; $\boldsymbol{F}^*$ is the dimensionless additional force and defined as

$$\boldsymbol{F}^* = \frac{2\pi\beta}{Re}\sin(2\pi y).$$

Besides, to simulate the fluid mixing, a transport equation of concentration field c is also solved after the flow has reached a statistically fully developed state, and given as

$$\frac{\partial c}{\partial t} + U\cdot\nabla c = \nabla^2 c/(Re\cdot Sc), \tag{4}$$

where *Sc* is the Schmidt number, defined as $Sc = (\eta_{\mathrm{P}}+\eta_{\mathrm{s}})/D$ with D being the mass diffusion coefficient of fluid.

The initial conditions for velocity and conformation fields in this study are obtained by converting those of the simulated 3D viscoelastic Kolmogorov flows[22] in a developed turbulent (elastic turbulence) state. For the spatial discretization of the momentum equations, a second-order central difference scheme is used, while a composite high solution scheme MINMOD is used for the convective term in the Giesekus constitutive equation and the concentration equation. For time advancing, the Adams–Bashforth scheme is used to guarantee a second-order accuracy in time. The pressure is obtained by solving the Poisson equation based on an implicit method. The details of the numerical procedures can be found in Ref. [7].

3. Results and discussion

In this simulation, the Reynolds numbers for all the cases are set to be 1 and so the channel flow of Newtonian fluid is definitely laminar. A sharp increase of the flow resistance or mean power injection is an important feature of the onset of elastic turbulence, and also a sign of transport enhancement of mass, momentum, and energy. The flow resistance is indirectly quantified by the momentum ratio between the elastic turbulent flow and a laminar flow of the Newtonian fluid at the same *Re*. By defining the momentum ratio $r = U_{\mathrm{l}}^2/U_e^2$, where U_{l} and U_{e} are the mean velocity amplitudes in the corresponding laminar flow and elastic turbulent flow, respectively, a sudden increase in r indicates the onset of elastic instability: flow resistance suddenly increases due to the onset of flow instability, in consequence the mean velocity amplitude also suddenly decreases, resulting in the sudden increase of r. Figure 2 shows the momentum ratio r and the ensemble root mean

square (RMS) of all the fluctuating velocity components E, defined as

$$E = \sqrt{\frac{1}{V}\iiint \left((u-\bar{u}_y)^2 + (v-\bar{v}_y)^2 + (w-\bar{w}_y)^2\right) \mathrm{d}V},$$

where V is the volume of the flow domain; $\bar{u}_y$, $\bar{v}_y$, and $\bar{w}_y$ represent the local mean velocity components at different y-locations in the streamwise, wall-normal and spanwise directions, respectively; note that, for laminar flow of Newtonian fluid, $E = 0$, each as a function of Wi. An abrupt increase of E can be observed when the Wi is above a certain critical value Wi_c, which is estimated to be 5 in this simulation. This symbolized the beginning of the transitional process from the laminar regime to an elastic instability, which can also be verified by the increase of r. From the curve of momentum ratio r, two transitional points (at $Wi = 5$ and 30, respectively) can be observed, which is qualitatively in agreement with the experimental results of elastic turbulence in curvilinear flows.[16] When Wi exceeds 5, the flow becomes unstable and the momentum ratio increases gradually; further, as Wi exceeds 30, a sudden increase of r is observed. A fully developed turbulent state of elastic turbulent flow can then be expected at a sufficiently large Wi though no simulation results are available now because of the breakdown of calculation at higher Wi numbers.

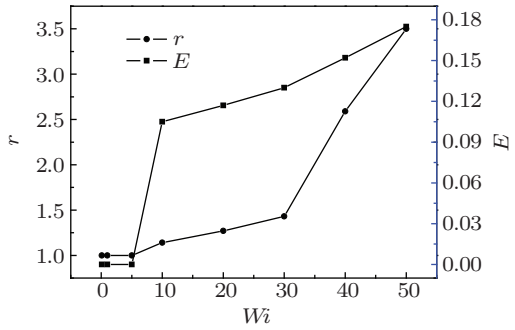


Fig. 2. Values of momentum ratio $r = U_e^2/U_l^2$ and ensemble root mean square of all the velocity components E each as a function of Wi, showing the onset of pure elastic turbulence.

The contributions of the viscous, elastic, and inertial stresses to the momentum budget are shown in Fig. 3. In the laminar regime ($Wi = 0$), the flow is dominated by the viscous stress. As Wi increases, the roles of viscous stress and elastic stress are exchanged. The elastic stress begins to grow at the transition Wi, and reaches a proportion much larger than the viscous contribution, and it is supposed to be dominant at a higher Wi. In elastic turbulence, the elastic stresses play similar roles to those the Reynolds stresses play in an inertial turbulence. Note interestingly that, at $Wi = 30$ when the sudden increase of momentum ratio r occurs (Fig. 2), the viscous and elastic stresses have just changed their roles played on the flow, i.e., the elastic stress just becomes larger than the viscous stress. It is then conjectured that the second transitional point appearing in Fig. 2 can be more precisely located at Wi right corresponding to the crossing point of the curves for viscous and elastic stresses as shown in Fig. 3 ($Wi \sim 28$). The contribution of inertial stress is always vanishingly small compared with the elastic contribution due to the small Re.

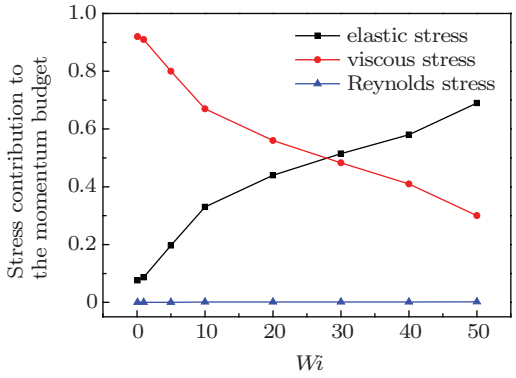


Fig. 3. (color online) Force balance among the elastic, viscous, and Reynolds stress (normalized by the amplitude of the additional force) as a function of Wi.

Another key feature of elastic turbulence is the strong extension of the microstructures existing in the viscoelastic solutions, which is usually represented by the trace of conformation tensor $\boldsymbol{C}$. Figure 4 shows the $\langle \mathrm{tr}(\boldsymbol{C})\rangle$, the mean trace of $\boldsymbol{C}$ at different Wi numbers. It can be seen that $\langle \mathrm{tr}(\boldsymbol{C})\rangle$ increases rapidly with Wi (linearly with a slope of about 13) above the critical value Wi_c, indicating that the microstructures are strongly stretched from the original coiled state.

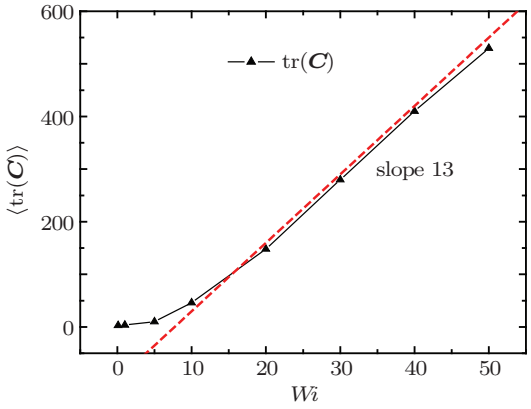


Fig. 4. (color online) $\langle \mathrm{tr}(\boldsymbol{C})\rangle$ as a function of Wi.

In this study, the added sinusoidal force to the momentum equation leads to a sinusoidal distribution of the mean streamwise velocity U_m (averaged in time and in the x–z plane) as shown in the inset of Fig. 5. Figure 5 displays the distributions of the root mean squares (RMS) of the three velocity components and velocity derivative ($\mathrm{d}u/\mathrm{d}y$) across the channel height, where

$$u_{\mathrm{rms}} = \sqrt{\frac{1}{A}\iint (u-\bar{u})^2 \mathrm{d}x\mathrm{d}z},$$

$$v_{\rm rms} = \sqrt{\frac{1}{A}\iint (v-\bar{v})^2 {\rm d}x{\rm d}z},$$

$$w_{\rm rms} = \sqrt{\frac{1}{A}\iint (w-\bar{w})^2 {\rm d}x{\rm d}z},$$

$$\left(\frac{{\rm d}u}{{\rm d}y}\right)_{\rm rms} = \sqrt{\frac{1}{\iint}\left(\frac{{\rm d}u}{{\rm d}y} - \frac{{\rm d}\bar{u}}{{\rm d}y}\right)^2 {\rm d}x{\rm d}z},$$

and A is the x–z plane area. As seen from the figure, there exist several small peaks in each RMS profile of velocity component corresponding to the local regions away from the top and bottom walls at which shear rates are large. This phenomenon is more evident in the RMS profile of velocity derivative shown in Fig. 5(b). The RMS of the streamwise velocity is much larger than those of the spanwise and wall-normal velocities because the sinusoidal force is applied in the streamwise direction. The maximum velocity fluctuation RMS can reach nearly 30% of amplitude of the mean velocity, suggesting that an unstable flow deviates far from the laminar regime, which can also be ascertained by the pictures of vorticity and the vortex structures illustrated in Fig. 6. We can see that the vorticity field distribution in the x–y plane shows streak-structures stretching in the streamwise direction (Fig. 6(a)), and the vortex tube structures are also elongated in the same direction (Fig. 6(b)). These could be attributed to the force added to the momentum equations. Due to the periodic additional force, the vorticity field distributed in the x–y plane can be divided into several similar layers including two near-wall layers along the wall-normal direction, and three layers of vortex structures formed in the corresponding positions that are also the exact regions where three significant peaks of RMS profile of velocity derivative emerge as shown in Fig. 5(b), namely the regions with great velocity gradients or large shear rates. Figure 6(c) shows the distribution of $\mathrm{tr}(\boldsymbol{C})/\langle \mathrm{tr}(\boldsymbol{C})\rangle$, trace of conformation tensor normalized by its mean value. It can be seen that the microstructures are strongly extended by the local velocity gradients mainly in the regions mentioned above. During the stretching process, energy is absorbed from the flow and stored in the microstructures, then the energy is transferred back to the flow through the relaxation of the microstructures after its saturation has been reached, finally unstable or even turbulent flow could be induced by such a process. Large velocity gradient or shear rate existing in the flow domain is essential for the extension of microstructures, which is related closely to the occurrence of elasticity-induced unstable or turbulent flow.

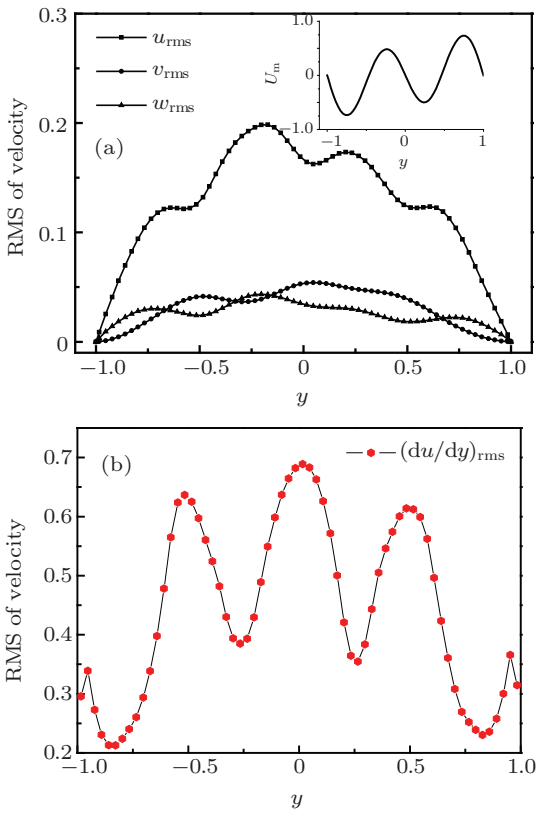


Fig. 5. (color online) Average values of RMS of velocity (a) and velocity derivative (b) in different x–z planes, $Wi = 30$. Inset of (a) is distribution of average velocity component u.

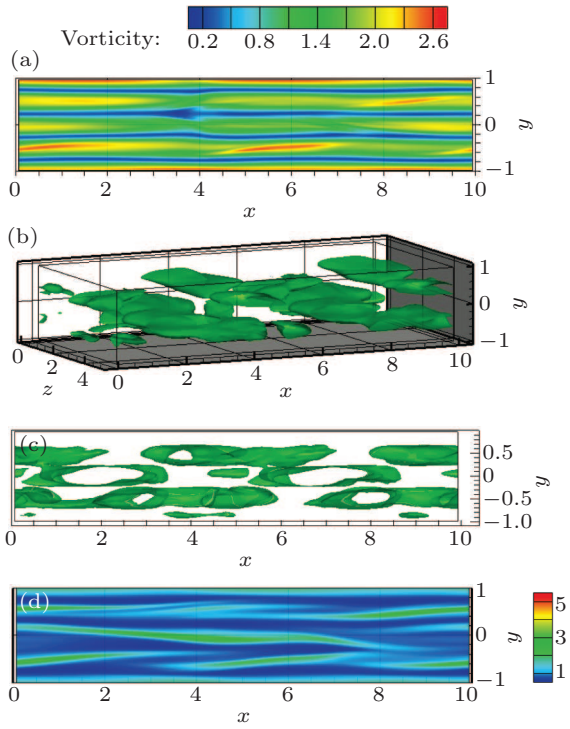


Fig. 6. (color online) Coherent structures and polymer extension in elastic turbulence, showing (a) vorticity field in the middle x–y plane, $Wi = 30$, (b) vortex structures obtained by a Q method, $Q = 0.1$ the upper is the 3D image, (c) the distribution of Q in the middle x–y plane, and (d) distribution of normalized extension $\mathrm{tr}(\boldsymbol{C})/\langle \mathrm{tr}(\boldsymbol{C})\rangle$ of microstructure in the middle x–y plane.

In order to give more evidence for turbulent characteristics of the flow and investigate the distributions of turbulent kinetic energy on different spatial scales, the power spectra of fluctuating velocity obtained in different x–z planes (one is near the wall at about $0.078h$, and the other is in the bulk flow region) are given in Fig. 7. As can be seen, the spectra each exhibit a broad range of power law decay with an exponent

about −4, confirming that turbulent fluid motions have been excited in a broad range of spatial scales. The exponent of the power law obtained in this study (−4), which is quite close to (but slightly smaller than) that given by Ref. [18] (−3.5) and that from simulation of a two-dimensional Kolmogorov flow[21] (−3.8), is much smaller than the power law exponent −5/3 at which the power of velocity fluctuation in inertial turbulence decays. This indicates that the turbulent energy in elastic turbulent flow is dissipated much more quickly than in inertial turbulence because of the effect of microstructures existing in the viscoelastic fluids. Furthermore, the power spectrum of fluctuating velocity near the wall is lower than that of the bulk flow, especially at larger wave numbers, which means that fluctuating velocity near the wall is smaller and decay is faster than those in the bulk flow. This is consistent with the distribution of RMS of velocity components displayed in Fig. 5. It is possibly attributed to the existence of the top and bottom walls, which stabilizes the chaotic motion of fluid locally, regardless of apparent polymers stretching.

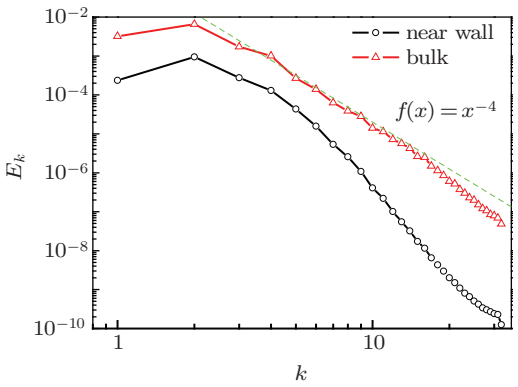


Fig. 7. (color online) Power spectra of fluctuating velocity in different x–z planes, $Wi = 30$.

Turbulent motion of the fluid is an irregular flow condition under which various quantities show a random variation with time and space coordinates. However, turbulence is not just a simple random motion and the flow intermittency is one of its salient features, which is also of great importance for fully understanding the mechanism of turbulent flow. The probability density function (PDF) and flatness factor $\beta = \langle\alpha^4\rangle/\langle\alpha^2\rangle^2$ of a random variable are the quantities often used to show the intermittency. If a flow is intermittent, the PDF of the velocity derivative will deviate from the Gaussian distribution, and the flatness will be larger than 3. Figure 8(a) shows the PDF of $\mathrm{d}u/\mathrm{d}y$ at a fixed point in the bulk flow. It shows that this PDF for elastic turbulence deviates from the Gaussian distribution, confirming the existence of intermittency in elastic turbulence also, which can also be verified by the flatness shown in Figs. 8(b) and 8(c). Figure 8(b) gives the flatness of $\mathrm{d}u/\mathrm{d}y$ along the wall-normal direction at different values of Wi's. As can be seen, there is nearly no intermittency in the flow when Wi is 10 (slightly higher than the transitional Wi_{cr}), at which the unstable flow is just induced. When the values of Wi are 20 and 40, the values of flatness are above 3 at almost all the positions, and become higher with the increase of Wi number, which means that the intermittency exists in most of the flow domain and turns stronger with Wi increasing. Furthermore, the intermittent behavior is a little stronger in boundary layers near the wall than in central regions of the channel. The values of flatness of velocity derivative $\mathrm{d}u/\mathrm{d}y$ each as a function of wave number k at $Wi = 40$ are presented in Fig. 8(c). The flatness is above 3 at most of the wave numbers except a few small wave numbers, and

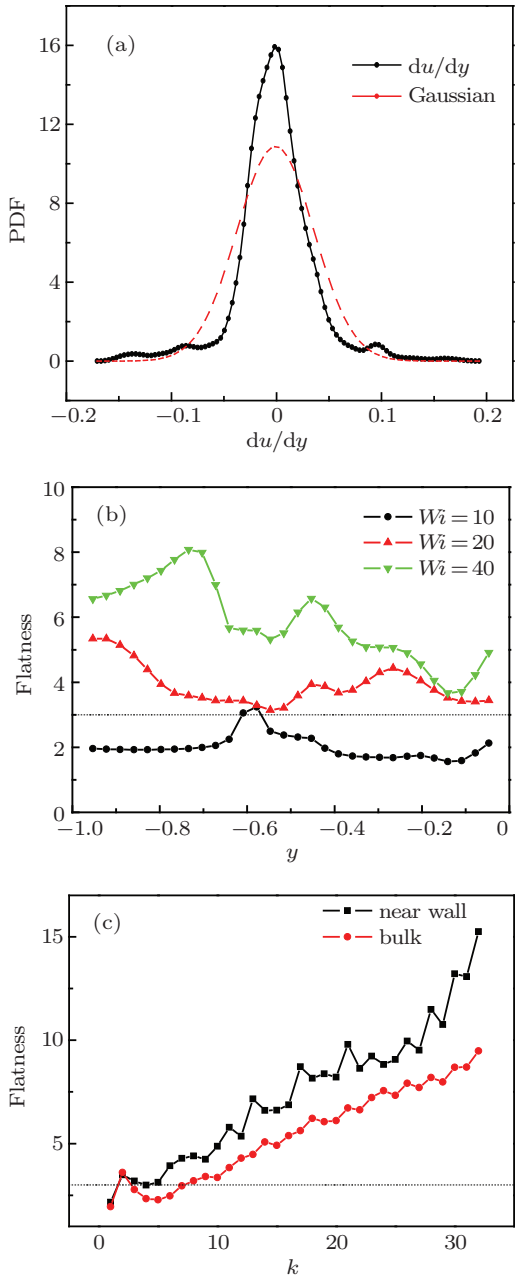


Fig. 8. (color online) Intermittent behavior of elastic turbulence, showing (a) PDFs of velocity derivatives, $Wi = 40$. (b) Flatness values of velocity derivatives each as a function of y coordinate, and (c) flatness factor each as a function of wave number k, $Wi = 40$.

becomes bigger with the increase of wave number k. It means that the intermittent behavior is excited on almost all the spatial scales, and is stronger on small spatial scales, which is similar to the case of inertial turbulence.

Since $Re = 1$, the channel flow of the Newtonian fluid is definitely restricted in stable laminar regimes, under which the convection of fluid is vanishingly weak and the transports of mass and energy rely mainly on the molecule diffusion. However, the unstable or turbulent flow of viscoelastic solution that can be excited at extremely low Re if Wi is large enough provides an effective way to enhance mass and energy transports. In our study, the transport equation of concentration c is solved to study the mixing enhancement effect. The initial value of concentration c is set to be 0 and 1 for the upper half and lower half region of the straight channel, respectively. The concentration c is then transported by the convection and diffusion of the flow. To estimate the mixing effect quantitatively, a mixing index is defined as RMS of c, i,e., $c_{\rm rms} = \sqrt{\sum_{i=1}^{N}(c_i - c_m)^2/N}$, where $c_{\rm m}$ is the average of initial c over the flow domain ($c_{\rm m} = 0.5$), and N is the number of grid points. The fluid is mixed uniformly if $c_{\rm rms}$ equals 0, while $c_{\rm rms} = 0.5$ corresponds to a completely unmixed condition. The distribution of c in a middle x–z plane of the channel at dimensionless time $t^* = 160$ is displayed in Fig. 9(b) to demonstrate the mixing results of viscoelastic solutions when elastic turbulence is induced as compared with the mixing of Newtonian fluid shown in Fig. 9(a). As displayed, the mixing effect of viscoelastic fluid flow is much better than that of Newtonian fluid flow (still clearly layered), because of the strong convection transport in elastic turbulence, which is absent in Newtonian fluid flow at low Re. The mixing index as shown in Fig. 9(c) descends rapidly with time going by for the viscoelastic fluid case, confirming the enhancement of mass transport by the elastic turbulent fluid motion, while for Newtonian fluid, the decrease of mixing index is extremely slow, suggesting a very weak mixing through molecule diffusion only.

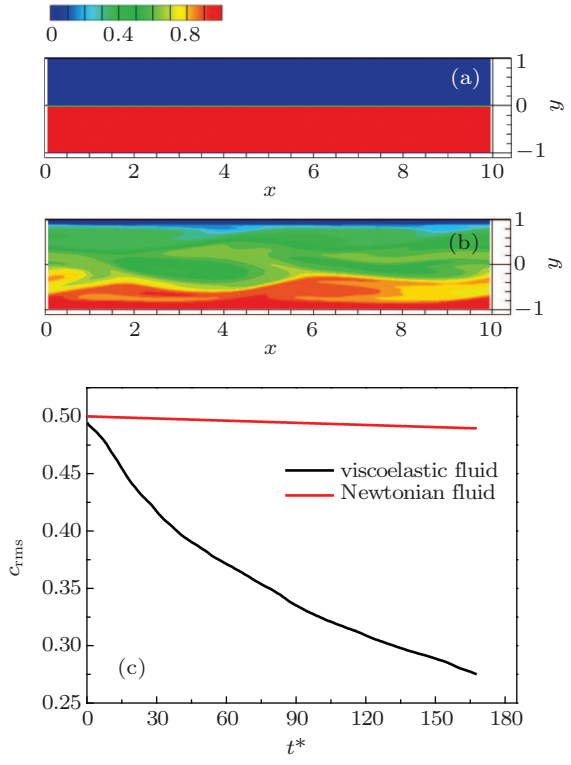


Fig. 9. (color online) Mixing of fluids in a straight channel, t*= 160, showing (a) contour of c for viscoelastic fluid at $Re = 1$ and $Wi = 30$, (b) contour of c for Newtonian fluid at $Re = 1$, and (c) mixing index $c_{\rm rms}$ as a function of dimensionless time t^*.

4. Conclusions

DNS of purely elastic turbulence in rectilinear shear flow in a 3D straight channel is presented for the first time in this paper. The elastic instability and elastic turbulence are realized in the straight channel with wall effect numerically by introducing a sinusoidal force term into the momentum equation for viscoelastic fluid flow and also into the Giesekus constitutive equation. It indicates that purely elastic instability and elastic turbulence can be induced in rectilinear shear flow as long as the Wi of viscoelastic flow is sufficiently high. The flow resistance (represented by the momentum ratio) and the root mean square of velocity components are found to increase abruptly when the elastic turbulence occurs. The vortex structures mainly lie in the regions where large shear rates or velocity gradients exist, and these are also the regions where the microstructures are strongly stretched. So the large shear rates are of great importance for generating the elastic turbulence. The elastic turbulent motion is excited in a broad range of spatial scale and the turbulent kinetic energy decays much faster than the inertial turbulence, with an exponent of -4 for the former as compared with $-5/3$ for the latter. Besides, the intermittency of elastic turbulence is also investigated by showing the PDF and flatness of the velocity derivative, indicating the flow exhibits intermittent behavior in most of the flow domain and in a large range of spatial scale provided that Wi is large enough, especially in the region near the wall. The potential application of elastic turbulence in enhancing fluid mixing is also demonstrated. A significant improvement on mixing efficiency is found compared with the laminar flow of Newtonian fluid at the same Reynolds number.

References

[1] Toms B A 1948 *Proc. 1st Int. Cong. Rheol.*, September 21–24, 1948, Scheveningen, Netherlands, p. 135
[2] Wei J J, Kawaguchi Y and Yu B 2008 *Chin. Phys. Lett.* **25** 4469
[3] Li F C, Kawaguchi Y, Segawa T and Hishida K 2004 *Phys. Fluids* **16** 3281
[4] Li F C, Kawaguchi Y, Segawa T and Hishida K 2005 *Phys. Fluids* **17** 075104
[5] Yu B and Kawaguchi Y 2004 *J. Non-Newtonian Fluid Mech.* **116** 431
[6] Li F C, Kawaguchi Y, Hishida K and Oshima M 2006 *Chin. Phys. Lett.* **23** 1226

[7] Cai W H, Li F C, Zhang H N, Li X B, Yu B, Wei J J, Kawaguchi Y and Hishida K 2009 *Phys. Fluids* **21** 115103
[8] Cai W H, Li F C and Zhang H N 2010 *J. Fluid Mech.* **665** 334
[9] Cai W H, Li F C, Zhang H N, Wang Y and Wang L 2012 *Sci. China* E **55** 854
[10] Cai W H, Li F C and Zhang H N 2011 *Chin. Phys.* B **20** 124702
[11] Li F C, Cai W H and Zhang H N 2012 *Chin. Phys.* B **21** 114701
[12] Groisman A and Steinberg V 2000 *Nature* **405** 53
[13] Burghelea T, Segre E and Steinberg V 2007 *Phys. Fluids* **19** 053104
[14] Groisman A and Steinberg V 2001 *Phys. Rev. Lett.* **86** 934
[15] Larson R G, Shaqfeh E S G and Muller S G 1990 *J. Fluid Mech.* **218** 573
[16] Groisman A and Steinberg V 2004 *New J. Phys.* **6** 29
[17] Burghelea T, Segre E, Bar-Joseph I, Groisman A and Steinberg V 2004 *Phys. Rev.* E **69** 066305
[18] Li F C, Kinoshita H, Li X B, Oishi M, Fujii T and Oshima M 2010 *Exp. Thermal & Fluid Sci.* **34** 20
[19] McKinley G H, Pakdel P and Oztekin A 1996 *J. Non-Newtonian Fluid Mech.* **67** 19
[20] Groisman A and Steinberg V 2001 *Nature* **410** 905
[21] Berti S, Bistagnino A, Boffetta G, Celani A and Musacchio S 2008 *Phys. Rev.* E **77** 055306
[22] Zhang H N, Li F C, Cao Y, Yang J C, Li X B and Cai W H 2011 *Proceedings of the* 6*th International Conference on Fluid Mechanics*, June 30–July 3, 2011, Guangzhou, China, p. 107
[23] Nghe P, Degre G, Tabeling P and Ajdari A 2008 *Appl. Phys. Lett.* **93** 204102
[24] Nghe P, Fielding S M, Tabeling P and Ajdari A 2010 *Phys. Rev. Lett.* **104** 248303